

FRET-based *in vivo* Ca²⁺ imaging by a new calmodulin-GFP fusion molecule

Kevin Truong¹, Asako Sawano^{2,3}, Hideaki Mizuno², Hiroshi Hama², Kit I. Tong¹, Tapas Kumar Mal¹, Atsushi Miyawaki² and Mitsuhiro Ikura¹

¹Division of Molecular and Structural Biology, Ontario Cancer Institute and Department of Medical Biophysics, University of Toronto, Toronto, Ontario M5G 2M9, Canada. ²Laboratory for Cell Function and Dynamics, Advanced Technology Development Center, Brain Science Institute, The Institute of Physical and Chemical Science (RIKEN), 2-1 Hirosawa, Wako-city, Saitama 351-0198, Japan. ³Brain Science Research Division, Brain Science and Life Technology Research Foundation, 1-28-12 Narimasu, Itabashi, Tokyo 175-0094, Japan.

Published online: 12 November 2001, DOI: 10.1038/nsb728

Intracellular Ca²⁺ acts as a second messenger that regulates numerous physiological cellular phenomena including development, differentiation and apoptosis. Cameleons, a class of fluorescent indicators for Ca²⁺ based on green fluorescent proteins (GFPs) and calmodulin (CaM), have proven to be a useful tool in measuring free Ca²⁺ concentrations in living cells. Traditional cameleons, however, have a small dynamic range of fluorescence resonance energy transfer (FRET), making subtle changes in Ca²⁺ concentrations difficult to detect and study in some cells and organelles. Using the NMR structure of CaM bound to the CaM binding peptide derived from CaM-dependent kinase kinase (CKKp), we have rationally designed a new cameleon that displays a two-fold increase in the FRET dynamic range within the physiologically significant range of cytoplasmic Ca²⁺ concentration of 0.05–1 μM.

The traditional yellow cameleon (YC)¹ consists of a tandem fusion of a cyan fluorescent protein (CFP)^{2,3}, CaM⁴, the CaM-binding peptide of myosin light chain kinase (MLCKp)⁵ and a yellow fluorescent protein (YFP)^{6–8}. Upon increasing the free Ca²⁺ concentration in solution, the CaM module of the cameleon binds Ca²⁺ and wraps around the fused MLCKp. This conformational change leads to a decrease in the distance between the two GFP variants and, therefore, an increase in FRET^{1,9}. By observing the change in the ratio of the fluorescence intensities of acceptor and the donor (R) in living cells, the onset and termination of Ca²⁺ signaling can be observed in a specific cellular compartment, such as the cytoplasm, nucleus or endoplasmic reticulum^{1,10}. One useful measure of the quality of an indicator is the dynamic range of the emission ratio, where dynamic range is defined as the maximum ratio, R_{max}, divided by the minimum ratio, R_{min}.

CaM-GFP-based Ca²⁺ indicators, such as cameleons and other engineered molecules^{11,12}, have many advantages over synthetic fluorescent dyes^{13–15}. Cameleons have been successfully expressed in certain cell types^{1,10} and can be targeted to specific organelles or sites for observation of local Ca²⁺ concentration changes. YC2.1 is a yellow cameleon¹ constructed from a YFP variant that is less sensitive to pH than the enhanced YFP (EYFP) in the original version of the Ca²⁺ indicator. Although YC2.1 has

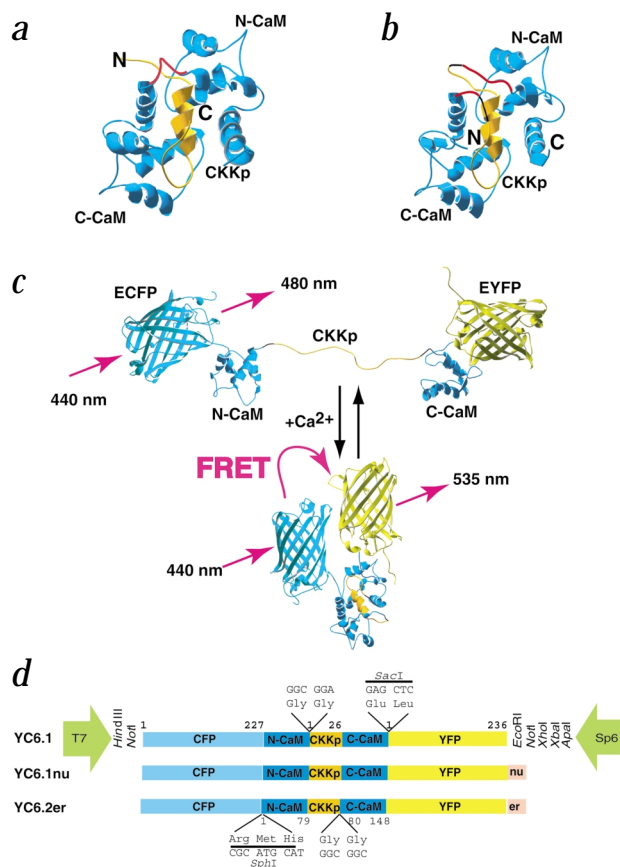


Fig. 1 Design of YC6.1. **a**, The ribbon diagram of CaM (blue) bound to CKKp (orange) shows that the CaM domain linker region (red) is near the N- and C-termini of CKKp. The CaM domain linker (residues 75–82) connects the N-terminal EF-hand Ca²⁺-binding domain (N-CaM) and the C-terminal EF-hand Ca²⁺-binding domain (C-CaM) of CaM. **b**, CKKp was inserted between CaM residues 79 and 80 and was connected to CaM via two Gly-Gly linkers (black). Consequently, two separate segments (75–79 and 80–82; red) of the original CaM linker remain in the fusion construct. The (N-CaM)-GG-CKKp-GG-(C-CaM) hybrid protein structure was modeled using MODELLER³³ and agrees with the experimentally solved CaM-CKKp complex in (a). **c**, A cartoon diagram illustrates how the conformation of YC6.1 might change from the Ca²⁺-free to Ca²⁺-saturated state. The GFP mutants are closer in the Ca²⁺-saturated state, thereby allowing FRET. **d**, Schematic diagram of YC6.1, YC6.1nu and YC6.2er. YC6.1 is a tandem fusion of CFP, N-CaM, CKKp, C-CaM and YFP. The gene can be excised using *HindIII* or *NotI* for the 5' end and *EcoRI*, *NotI*, *XhoI*, *XbaI* or *Apal* for the 3' end. In addition to this cytoplasmic version of YC6.1, nucleus- and endoplasmic reticulum-targeting versions of YC6.1 (YC6.1nu and YC6.2er, respectively) have been constructed.

a reported dynamic range of about two between zero and saturating Ca²⁺ concentrations *in vitro*, the change in the emission ratio is only 1.6-fold *in vivo*⁹. A more effective *in vivo* Ca²⁺ indicator would have a larger dynamic range so that signal and noise can be easily distinguished, but still maintain the advantages of cameleons.

Structure-based design of a new cameleon

In order to improve the dynamic range of cameleons, we constructed a new yellow cameleon, YC6.1, based on the structure of CaM in complex with CKKp¹⁶. In contrast to the design of YC2.1, which was based on the structure of CaM bound to MLCKp where CaM is fused to MLCKp at the C-terminus¹⁷, our structural studies on the CaM-CKKp complex¹⁶ suggested that the CaM binding peptide could be fused at the linker region

letters

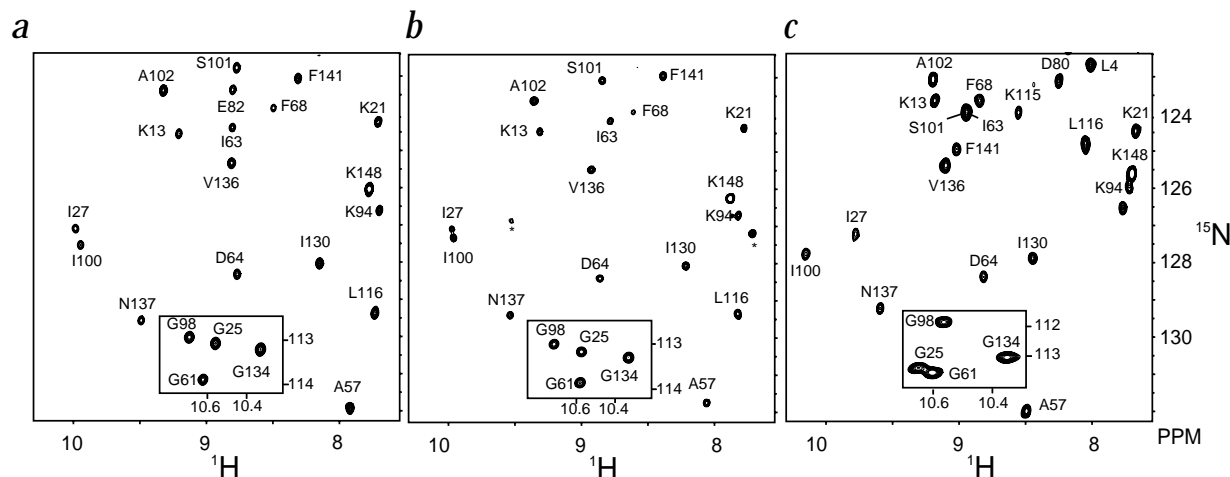


Fig. 2 ^1H - ^{15}N HSQC NMR spectra of ^{15}N labeled CaM in complex with CKKp and ^{15}N labeled (N-CaM)-CKKp-(C-CaM). Portion of the ^1H - ^{15}N HSQC spectrum of **a**, ^{15}N -uniformly-labeled CaM complex with CKKp; **b**, ^{15}N -uniformly-labeled (N-CaM)-CKKp-(C-CaM); and **c**, ^{15}N -uniformly-labeled CaM, all in the presence of 10 mM CaCl_2 . For clarity, only part of the spectrum is shown, including the most downfield shifted glycine region of the spectrum (in the inset box). The resonances labeled with an asterisk in spectrum (**b**) represent the backbone amides from the CKKp portion of the hybrid. Note that residue Glu 82 is missing from spectrum (**b**) due to its close proximity to the fusion site. (**b**) is similar to (**a**) and different from (**c**), as is expected for a hybrid construct folding in to a CaM-CKKp-like complex.

between the N- and C-terminal domains of CaM (Fig. 1a,b). This construction was possible given the unique CaM-binding mode of CKKp, which differs from that observed in MLCKs^{5,18} and CaMKII¹⁹. Whereas the MLCK and CaMKII peptides adopt α -helical conformations only in the CaM-binding region, CKKp assumes a fold comprising an α -helix and a hairpin-like loop, both of which are essential for the intimate interaction with CaM. In this complex, both the N- and C-termini of CKKp are oriented toward the linker region that connects the two EF-hand domains (Fig. 1a). Furthermore, the binding orientation of CKKp with respect to the two CaM domains is opposite to that of the MLCK and CaMKII peptides; thus, the N-terminus is also near the linker region of CaM. This analysis

suggests that CKKp could replace the CaM linker region. We have constructed YC6.1 by a tandem fusion of CFP, the N-terminal fragment of CaM (N-CaM), Gly-Gly, CKKp, Gly-Gly, the C-terminal fragment of CaM (C-CaM) and YFP (Fig. 1d).

To increase the dynamic range, the change in the distance between fluorophores must be large between the Ca^{2+} -free and the Ca^{2+} -bound states. For the CaM-MLCKp hybrid¹⁷ used in YC2.1 and YC3.1 (refs 1,10), the distance from the amino group of the N-terminus residue of CaM to the carboxyl group of the C-terminus of MLCKp is 50–60 Å, an estimate of the distance between the fused GFP variants. In contrast, in the structure of CaM bound to CKKp¹⁶, the distance between the N- and C-termini of CaM is significantly shorter than 40 Å. Assuming that, in the absence of Ca^{2+} , the fluorescent protein modules are separated by a similar distance in these two constructs and FRET efficiency is inversely proportional to the sixth power of the separation distance^{20,21}, a 20 Å or larger difference could, in principle, produce a marked increase in FRET for the Ca^{2+} -bound state (high R_{max}).

Global conformation

To test whether our design was successful, we studied the (N-CaM)-CKKp-(C-CaM) fusion protein by NMR spectroscopy. ^1H - ^{15}N heteronuclear single quantum coherence (HSQC) spectra (Fig. 2) provide evidence that the Ca^{2+} -loaded (N-CaM)-CKKp-(C-CaM) hybrid forms the compact global conformation similar to that observed in the solution structure of the Ca^{2+} -CaM-CKKp complex¹⁶. In the presence of Ca^{2+} , the two spectra are nearly identical, except that in the HSQC spectrum of the ^{15}N -labeled hybrid molecule, the crosspeaks from the CKKp portion, as well as the Gly-Gly linkers, are clearly observed. In the CaM-CKKp complex, the peptide was not

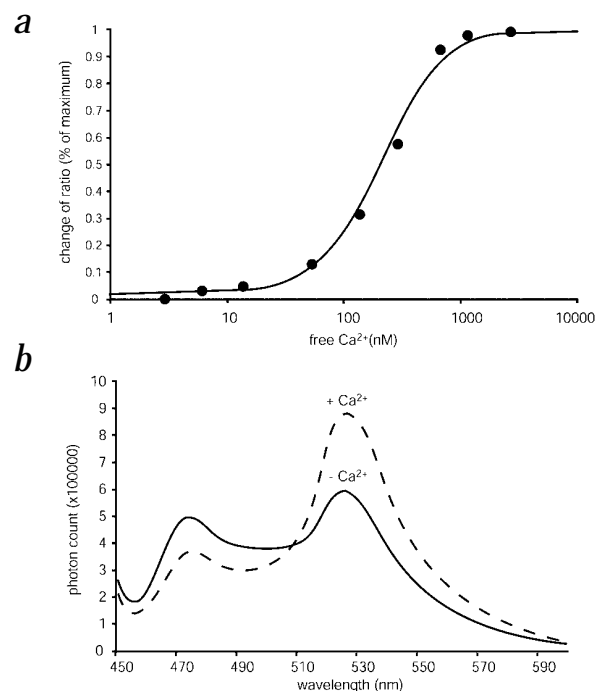


Fig. 3 Fluorescence properties of YC6.1 *in vitro*. **a**, The Ca^{2+} titration curve of YC6.1 was acquired using Ca^{2+} /EGTA and Ca^{2+} /EGTA-OH systems³⁰ below 10^{-5} M free Ca^{2+} in a 50 mM HEPES/KOH, pH 7.4, and 100 mM KCl buffer. The changes in emission ratio (530–480 nm) were normalized to the effects of full Ca^{2+} saturation. **b**, Emission spectrum of YC6.1 *in vitro* was acquired at an excitation wavelength of 432 nm for zero (1 mM EGTA) and saturating Ca^{2+} concentrations (5 mM CaCl_2).

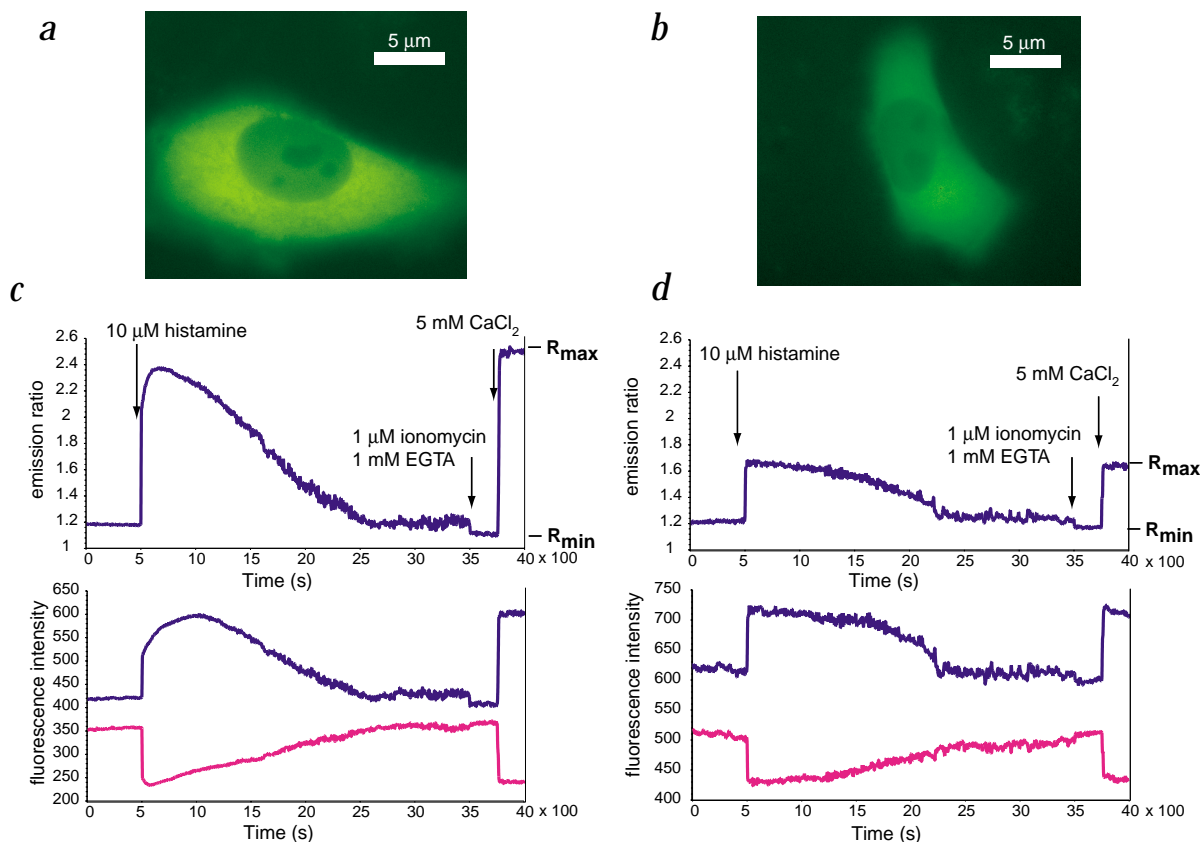


Fig. 4 Ca^{2+} imaging of HeLa cells using YC2.1 and YC6.1. **a, b**, The fluorescence image (440 ± 10 nm excitation, 535 ± 12.5 nm emission) in HeLa cells show cytoplasmic localization of YC6.1 and YC2.1, respectively. **c, d**, The HeLa cells were stimulated with $10 \mu\text{M}$ histamine. The emission ratios (from 535 ± 12.5 nm to 480 ± 12.5 nm) and intensities (535 ± 12.5 nm and 480 ± 12.5 nm) of the cells were measured every 5 s by digital imaging microscopy for both YC6.1 and YC2.1, respectively. The right-hand axes of the top graphs are labeled with R_{\min} and R_{\max} .

labeled with ^{15}N and, thus, no signal from the peptide is detected in the HSQC spectrum.

In the absence of Ca^{2+} , the HSQC spectra of the CaM-MLCKp hybrid display a broadening of some peaks¹⁷, suggesting that the MLCKp interacts with CaM under this condition. A similar phenomenon was observed when CKKp was fused to the N-terminus of CaM (K.I.T. & M.L., unpublished results). This interaction is undesirable for our FRET applications, because it would increase R_{\min} , thereby reducing the dynamic range. The spectra of the Ca^{2+} -free (N-CaM)-CKKp-(C-CaM) hybrid, however, showed no significant broadening (data not shown), suggesting that two CaM domains have little interaction with CKKp. These NMR data strongly support the idea that the (N-CaM)-CKKp-(C-CaM) hybrid has a greater separation distance in the Ca^{2+} -free state than the CaM-MLCKp, and that Ca^{2+} binding to the hybrid induces a large conformational change resulting in the compact global conformation, bringing CFP and YFP spatially close together within YC6.1 (Fig. 1c).

Ca^{2+} binding properties

YC2.1 displayed a biphasic Ca^{2+} binding curve with two apparent dissociation constants (100 nM and $4.3 \mu\text{M}$)¹⁰ due to the two conformational states of the construct¹⁷. This property has been considered to be one of the desired characteristics of YC2.1 (ref. 1) because it can respond to a wide range of free Ca^{2+} concentrations from 0.01 to $100 \mu\text{M}$. In contrast, YC6.1 possesses a monophasic Ca^{2+} binding curve with a single apparent dissociation

constant of 110 ± 6 nM and, therefore, responds to free Ca^{2+} concentrations ranging from 0.05 to $1 \mu\text{M}$ in a more linear manner than YC2.1 (Fig. 3a).

In an unstimulated eukaryotic cell, the concentration of free Ca^{2+} ions in the cytoplasm ($[\text{Ca}^{2+}]_c$) is approximately $0.1 \mu\text{M}$ and rises to $1 \mu\text{M}$ following stimulation²². It is, therefore, advantageous to have an indicator with enhanced coverage in this physiologically relevant range of $[\text{Ca}^{2+}]_c$. Although YC2.1 covers a larger range of free Ca^{2+} concentration than YC6.1, the emission ratio change of YC2.1 is distributed across this entire Ca^{2+} range; therefore, a smaller dynamic range is available for applications focused on specific Ca^{2+} concentrations. In contrast, the dynamic range of YC6.1 applies to the cytoplasmic free Ca^{2+} concentrations. Thus, both its Ca^{2+} binding and fluorescence characteristics should make YC6.1 a more suitable indicator than YC2.1 in some *in vivo* imaging applications.

Ca^{2+} imaging in HeLa cells

To characterize the performance of YC6.1 *in vivo* and to compare it with that of YC2.1, we imaged HeLa cells transfected with the cameleons. In the cells expressing either YC6.1 or YC2.1, the fluorescence from the cameleons was uniformly distributed in the cytoplasm but excluded from the nucleus (Fig. 4a,b), as expected for a 72.6 kDa protein without targeting signals. After histamine stimulus, the time course of the spatially-averaged emission fluorescence intensities was measured in single HeLa cells expressing YC6.1 (Fig. 4c) and YC2.1 (Fig. 4d). The binding

letters

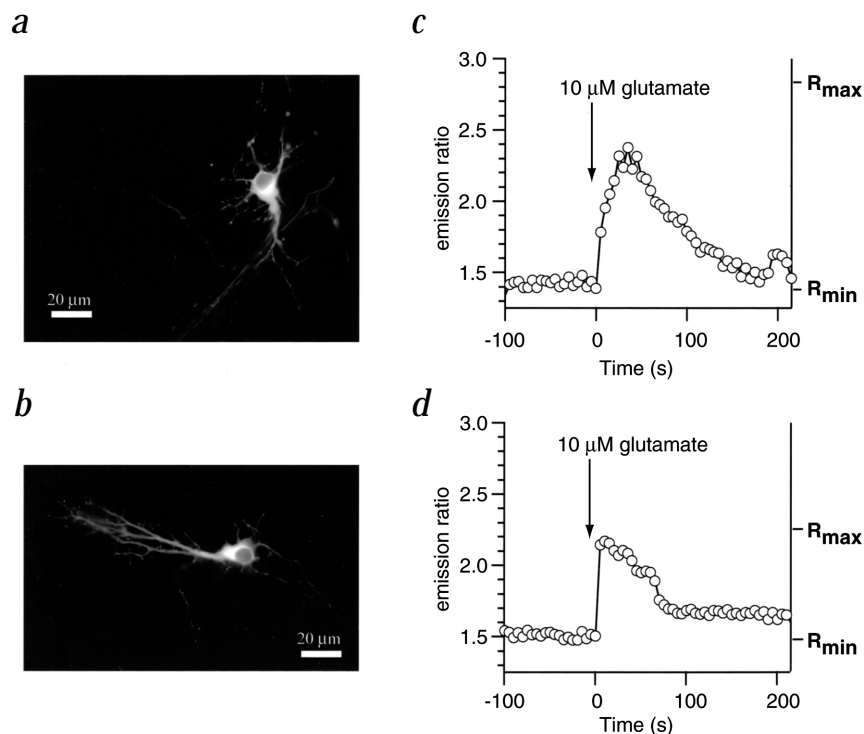


Fig. 5 Ca^{2+} imaging of rat hippocampus neurons using YC2.1 and YC6.1. **a,b**, The fluorescence image in neuronal cells also shows cytoplasmic localization of YC6.1 and YC2.1, respectively. **c,d**, The neuronal cells were stimulated with 10 μM glutamate. The emission ratios and intensities of the cells were measured for both YC6.1 and YC2.1, respectively.

of histamine to its receptors on the plasma membrane sets off a signaling cascade, resulting in Ca^{2+} release from the endoplasmic reticulum through the inositol-1,4,5-triphosphate receptor (InsP_3R). Prior to stimulus, the emission ratio was constant (signifying a steady state of $[\text{Ca}^{2+}]_i$); however, upon addition of 10 μM histamine, there was a sharp rise in emission ratio (signifying an increase in $[\text{Ca}^{2+}]_i$)^{23,24}. The increase of YFP and the decrease of CFP fluorescence intensities indicate an increase in FRET resulting from a conformational change. YC6.1 displayed a slower increase in emission ratio following stimulation when compared to YC2.1, suggesting that YC6.1 may have slower activation kinetics. After ~ 30 min, the histamine response dissipated and both $[\text{Ca}^{2+}]_i$ and emission ratio returned to their steady state levels. To obtain R_{\min} , the emission ratio was measured after adding 1 μM Ca^{2+} ionophore ionomycin and 1 mM EGTA; to obtain R_{\max} , another measurement was made after adding 5 mM CaCl_2 to the same sample. Under these experimental conditions, the emission ratio of YC2.1 changed from 1.17 ± 0.01 (R_{\min}) to 1.66 ± 0.01 (R_{\max}), whereas the ratio of YC6.1 doubled from 1.18 ± 0.01 (R_{\min}) to 2.50 ± 0.02 (R_{\max}). Given this enhanced FRET dynamic range, the $[\text{Ca}^{2+}]_i$ before and after histamine addition were estimated to be ~ 43 nM and ~ 1 μM , respectively, by mapping the change in emission ratio to Fig. 3a.

The increase in the FRET dynamic range of YC6.1 over YC2.1 is somewhat lower than anticipated based on the shorter distance between the CFP and YFP chromophores originally predicted from the structure-based design of YC6.1. This is not surprising because the intrinsic FRET efficiency also depends on the relative orientation of the donor and acceptor chromophores²⁵, which is difficult to predict from the available structural data. Other factors influencing the observed emission ratio between 485 and 535 nm include folding and chromophore maturation efficiency of the GFP fusion constructs²⁶ as well as the pH sensitivity of the GFP emission intensity⁹; these often differ from one construct to another. Nevertheless, YC6.1 consistently displayed a two-fold increase in the FRET dynamic range within

the physiologically significant range of cytoplasmic Ca^{2+} concentration (0.05–1 μM).

Ca^{2+} imaging in hippocampal neurons

Ca^{2+} signaling was also tested in rat hippocampal neurons, where it has been shown that glutamate stimulates an increase of $[\text{Ca}^{2+}]_i$ through the N-methyl-D-aspartate (NMDA) receptor²⁷. YC2.1 and YC6.1 were expressed in isolated rat hippocampal neurons where transient changes in $[\text{Ca}^{2+}]_i$ were induced by application of 10 μM glutamate (Fig. 5). Following stimulation, a post-synaptic Ca^{2+} spike lasting ~ 3 min was observed in both YC6.1- and YC2.1-expressing neurons. The dynamic range of the Ca^{2+} -dependent emission ratio change of cameleons were compared in the YC6.1- and YC2.1-expressing neurons (Fig. 5a,b). Whereas the dynamic range was ~ 1.6 for YC2.1, YC6.1 reproducibly exhibited an almost two-fold emission ratio change. The pre- and post-glutamate $[\text{Ca}^{2+}]_i$ in hippocampal cells was estimated, in a similar way as in the HeLa cells, to be ~ 28 nM and ~ 550 nM, respectively. The improved dynamic range allows us to better distinguish between signal and noise from intracellular $[\text{Ca}^{2+}]$ changes.

Conclusions

The three-dimensional structure of CaM in complex with MLCKp has previously provided a template for constructing original cameleons such as YC2.1 and YC3.1 (refs 1,10). Here we present a second generation of the cameleon family of Ca^{2+} indicators designed using the CaM-CKKp structure¹⁶ as a new template. The unique CaM binding mode of CKKp suggests that it could replace the CaM domain linker region without significantly affecting the overall conformation of the CaM-CKKp complex. As a result, the distance between CFP and YFP chromophores attached to the N- and C-termini of the CaM-CKKp fusion protein is reduced by ~ 20 Å relative to that of the CaM-MLCKp version. In *in vivo* imaging, this new design results in a two-fold enhancement in the FRET efficiency, thereby



expanding the ability of cameleons to visualize Ca^{2+} mobilization in living cells where a high sensitivity is required for detection. Clearly, the structural diversity in CaM-target recognition²⁸ offers a variety of design opportunities in CaM-based protein engineering aimed at improved *in vivo* Ca^{2+} indicators.

Methods

Gene construction. A DNA fragment (fragment A) encoding *Xenopus laevis* CaM (xCaM) Glu 7–Thr 79 (N-CaM) fused to rat calmodulin dependent protein kinase kinase (rCKK) Val 438–Phe 463 (ref. 16) and xCaM Asp 80–Lys 148 (C-CaM) was generated by gene splicing using PCR techniques²⁹. Two short segments encoding Gly-Gly linkers were inserted between N-CaM and the rCKK peptide (CKKp), and between CKKp and C-CaM (Fig. 1d). Two restriction sites, *SphI* and *SacI*, were introduced by standard PCR method into the 5' and 3' ends, respectively, of fragment A. To construct YC6.1, the *BamHI/EcoRI* or the *HindIII/EcoRI* gene fragments encoding YC2.1 in the expression vectors of pRSETb or pcDNA3 (refs 1,10), respectively, were spliced into pUC19 via the corresponding restriction sites. Using these pUC19 intermediate constructs, the fragment encoding CaM-MLCKp of YC2.1 was replaced by fragment A via the *SphI/SacI* sites. This recombinant gene was then transferred back to pRSETb or pcDNA3 expression vectors via *BamHI/EcoRI* or *HindIII/EcoRI* sites, respectively.

Protein expression, *in vitro* spectroscopy and Ca^{2+} titrations. Chimeric proteins were expressed in *Escherichia coli*, purified and spectroscopically characterized as described³. Ca^{2+} titrations were performed by reciprocal dilution of Ca^{2+} -free and Ca^{2+} -saturated buffers³⁰.

NMR Measurements. ^1H - ^{15}N HSQC spectra were recorded on a Varian INOVA Unity-plus 600 MHz spectrometer equipped with a triple-resonance, pulse field gradient probe with an actively shielded z-gradient and a gradient amplifier unit, using the pulse scheme described elsewhere³¹. All spectra were recorded with 256 complex t_1 increments of 1K complex data points and 16 transients. Spectral widths were 30 ppm and 15 ppm for the ^{15}N (F_1) and ^1H (F_2) dimensions. The spectra were recorded at pH 6.8, 32 °C, in 90/10% (v/v) $\text{H}_2\text{O}/\text{D}_2\text{O}$. The sample concentration is approximately 1.2 mM. The data were processed using NMRPipe.

Imaging. HeLa cells were transfected with lipofectin (Gibco BRL), whereas hippocampus neurons were transfected with a Ca^{2+} phosphate procedure³². Between two and five days after transfection, cells were imaged at 22 °C on an Olympus IX70 microscope with a CCD camera (MicroMax 1300YHS) controlled by MetaFluor 4.5r2 software (Universal Imaging). Dual-emission ratio imaging of yellow cameleons used a 440DF20 excitation filter, a 455DRLP dichroic

mirror and two emission filters (480DF30 for CFP, 535DF25 for YFP) alternated by a filter changer (Lambda 10-2, Sutter Instruments). Interference filters were obtained from Omega Optical (Brambleboro).

Acknowledgments

This work was supported in part by a grant from Howard Hughes Medical Institute (HHMI) to M.I., CREST (Core Research for Evolutional Science and Technology) and an NCIC Fellowship to T.K.M.. M.I. is an HHMI International Scholar and a Canadian Institutes of Health Research Scientist. We thank J. Gooding for her excellent assistance in manuscript editing. The YC6 vectors are available from the authors upon request.

Correspondence should be addressed to M.I. email: mikura@uhnres.utoronto.ca

Received 24 July, 2001; accepted 10 October, 2001.

1. Miyawaki, A. *et al. Nature* **388**, 882–887 (1997).
2. Heim, R., Prasher, D.C. & Tsien, R.Y. *Proc. Natl. Acad. Sci. USA* **91**, 12501–12504 (1994).
3. Heim, R. & Tsien, R.Y. *Curr. Biol.* **6**, 178–182 (1996).
4. Crivici, A. & Ikura, M. *Annu. Rev. Biophys. Biomol. Struct.* **24**, 85–116 (1995).
5. Ikura, M. *et al. Science* **256**, 632–638 (1992).
6. Heim, R., Cubitt, A.B. & Tsien, R.Y. *Nature* **373**, 663–664 (1995).
7. Cormack, B.P., Valdivia, R.H. & Falkow, S. *Gene* **173**, 33–38 (1996).
8. Ormo, M. *et al. Science* **273**, 1392–1395 (1996).
9. Miyawaki, A. & Tsien, R.Y. *Methods. Enzymol.* **327**, 472–500 (2000).
10. Miyawaki, A., Griesbeck, O., Heim, R. & Tsien, R.Y. *Proc. Natl. Acad. Sci. USA* **96**, 2135–2140 (1999).
11. Nagai, T., Sawano, A., Park, E.S. & Miyawaki, *Proc. Natl. Acad. Sci. USA* **98**, 3197–3202 (2001).
12. Baird, G.S., Zacharias, D.A. & Tsien, R.Y. *Proc. Natl. Acad. Sci. USA* **96**, 11241–11246 (1999).
13. Tsien, R. & Pozzan, T. *Methods. Enzymol.* **172**, 230–262 (1989).
14. Tsien, R.Y., Rink, T.J. & Poenie, M. *Cell Calcium* **6**, 145–157 (1985).
15. Wahl, M., Lucherini, M.J. & Gruenstein, E. *Cell Calcium* **11**, 487–500 (1990).
16. Osawa, M. *et al. Nature Struct. Biol.* **6**, 819–824 (1999).
17. Porumb, T., Yau, P., Harvey, T.S. & Ikura, M. *Protein Eng.* **7**, 109–115 (1994).
18. Meador, W.E., Means, A.R. & Quijcho, F.A. *Science* **257**, 1251–1255 (1992).
19. Meador, W.E., Means, A.R. & Quijcho, F.A. *Science* **262**, 1718–1721 (1993).
20. Stryer, L. *Annu. Rev. Biochem.* **47**, 819–846 (1978).
21. Truong, K. & Ikura, M. *Curr. Opin. Struct. Biol.* **11**, 573–578 (2001).
22. Berridge, M.J., Lipp, P. & Bootman, M.D. *Nature Rev. Mol. Cell Bio.* **1**, 11–21 (2000).
23. Zamani, M.R. & Bristow, D.R. *Brit. J. Pharmacol.* **118**, 1119–1126 (1996).
24. Bootman, M.D., Cheek, T.R., Moreton, R.B., Bennett, D.L. & Berridge, M.J. *J. Biol. Chem.* **269**, 24783–24791 (1994).
25. Forster, T. *Ann. Physik.* **2**, 55–75 (1948).
26. Waldo, G.S., Standish, B.M., Berendzen, J. & Terwilliger, T.C. *Nature Biotech.* **17**, 691–695 (1999).
27. Blackstone, C. & Sheng, M. *Cell Calcium* **26**, 181–192 (1999).
28. Yap, K. *et al. J. Struct. Funct. Genomics* **1**, 8–14 (2000).
29. Horton, R.M., Hunt, H.D., Ho, S.N., Pullen, J.K. & Pease, L.R. *Gene* **77**, 61–68 (1989).
30. Grynkiewicz, G., Poenie, M. & Tsien, R.Y. *J. Biol. Chem.* **260**, 3440–3450 (1985).
31. Kay, L.E., Keifer, P. & Saarinen, T. *J. Am. Chem. Soc.* **114**, 10663–10665 (1992).
32. Wigler, M., Pellicer, A., Silverstein, S. & Axel, R. *Cell* **14**, 725–731 (1978).
33. Sanchez, R. & Sali, A. *Methods Mol. Biol.* **143**, 97–129 (2000).